

## AN OMNIDIRECTIONAL STEREO VISION SYSTEM

**Eduardo Lobo Lustosa Cabral** (\*), [elcabral@usp.br](mailto:elcabral@usp.br) / [elcabral@maua.br](mailto:elcabral@maua.br)

**Paulo Roberto Godoi de Oliveira**, [paulo.godoi@poli.usp.br](mailto:paulo.godoi@poli.usp.br)

Depto. de Eng. Mecatrônica e de Sist. Mecânicos – Escola Politécnica da USP / (\*) Escola de Eng. Mauá – CEUN-IMT  
Av. Prof. Mello Moraes, 2231 – 05508-900 São Paulo, SP, Brasil / (\*) Pr. Mauá,1 – 09580-900, S.C. doSul, SP, Brasil

**José Carlos de Souza Junior**, [jcarlos@maua.br](mailto:jcarlos@maua.br)

Escola de Engenharia Mauá - Centro Universitário do Instituto Mauá de Tecnologia  
Praça Mauá, 1 – 09580-900, São Caetano do Sul, SP, Brasil

**Abstract.** *This paper presents a new approach to design a panoramic stereo vision system based on a double lobed mirror with hyperbolic profile. The vision system may be used for 3D reconstruction or for obtaining range estimations in a form appropriated for mobile robot navigation. As hyperbolic mirrors ensure a single viewpoint the incident light rays are easily found from the points of the image. The geometry of the double lobed mirror naturally ensures matched epipolar lines in the two images of the scene. These two properties make the vision system based on the double lobed mirror especially suitable for panoramic stereo vision because 3D reconstruction becomes simple and fast. This is a great advantage for real-time applications. An error analysis for the calculated ranges is performed to provide information for the design of the omnidirectional vision system. Results show that the system is able to calculate range of objects with the necessary accuracy for robot navigation.*

**Keywords:** *Omnidirectional vision, stereo vision, double lobed mirror, hyperbolic mirror*

### 1. INTRODUCTION

Panoramic imaging is an important tool in machine vision and it is widely used in the area of mobile robots, see for instance (Koyasu et al., 2002; Delahoche et al., 2000). Among the many possible types of panoramic vision systems an attractive approach is to mount a single fixed camera under a mirror covering a hemisphere. These systems are normally referred as catadioptric. The advantages of a catadioptric system are the wide angle of view, and the fast acquisition rate. However, a disadvantage is that the images acquired have a relatively low spatial resolution. The shape of the mirror determines the image formation model of a catadioptric panoramic system. Different mirror shapes have been used and tested see for instance (Gaspar et al., 2002; Yamazawa et al., 1999; Conroy and Moore, 1999). A catadioptric system based on a hyperbolic mirror and a perspective (pinhole) camera forms an omnidirectional vision system with a single effective viewpoint. This characteristic is especially suitable for stereo imaging because the incident light rays are easily determined from the points of the image.

Another important tool for mobile robots and machine vision is stereo vision. Stereo vision allows determining the range to objects within the field of view of the system. Panoramic stereo vision is very convenient because the field of view is 360°.

Omnidirectional systems based on hyperbolic mirrors have been used for stereo vision as reported in (Koyasu et al., 2002; Gluckman et al., 1998). However, such systems were developed based on two mirrors and two cameras. Besides these systems are not compact they have the problem of requiring precise positioning of the cameras and the mirrors to guarantee perfect alignment of the images.

Panoramic stereo based on a double lobed mirror was first suggested by Southwell et al. (1996). A double lobed mirror is essentially a coaxial mirror pair, where the centers of both mirrors are collinear with the camera axis, and the mirrors have a symmetric profile around this axis. This arrangement has the great advantage to produce two panoramic views of the scene in a single image. A resolution invariant double lobed mirror was developed by Yamazawa et al. (1999), however, a catadioptric stereovision system based on a constant resolution mirror is not adequate for fast range estimation or three-dimensional stereo reconstruction since it requires solving a non-linear differential equation to obtain the mirror shape function and its slope at the reflection point.

This paper presents a new stereo vision system based on a catadioptric system with a hyperbolic double lobed mirror. The single viewpoint and the alignment of the images ensuring matched epipolar lines make this system ideal for fast real-time stereo calculations. Accurate range estimations are obtained at distances far enough to allow this system to be used for mobile robot navigation and 3D reconstruction.

### 2. THE OMNIDIRECTIONAL STEREO VISION SYSTEM

The omnidirectional stereo vision system is composed by a conventional perspective (pinhole) camera aligned vertically (coaxially) with the hyperbolic double lobed mirror. Fig. 1 presents a schematic of the system showing the field of view of the two mirror sections.

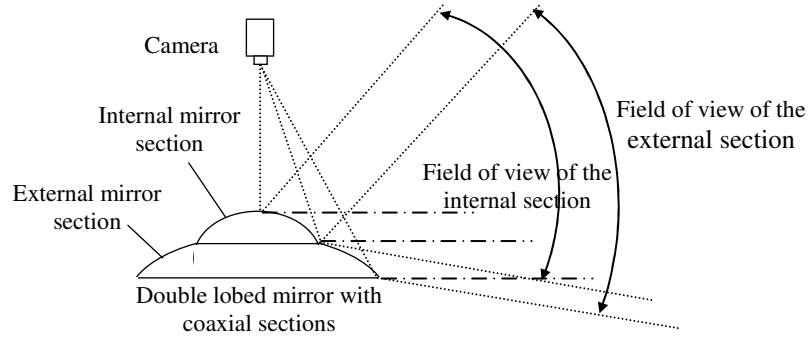


Figure 1. The omnidirectional stereo vision system based on a double lobed mirror.

### 2.1. The hyperbolic double lobed mirror

Due to the rotational symmetry of the system only the radial cross section of the mirror need to be considered. Figure 2 presents a schematic of the omnidirectional stereo vision system showing two incident and reflective light rays on the two mirror lobes.

A perspective camera together with a hyperbolic mirror form a wide-angle imaging system with two centers of projections, located at the hyperbole focal points. In Fig. 2 points  $F_0$  and  $F_I$  are the two focal points of the internal lobe hyperbolic mirror, and points  $F_0$  and  $F_E$  are the focal points of the external lobe hyperbolic mirror. All incident light rays on the internal lobe mirror pass through focal point  $F_I$  and it is reflected passing the other focal point  $F_0$ . Similarly, all incident light rays on the external lobe mirror pass through focal point  $F_E$  and are reflected passing the other focal point  $F_0$ . The internal and external hyperbole focus  $F_0$  must coincide with the camera focal center.

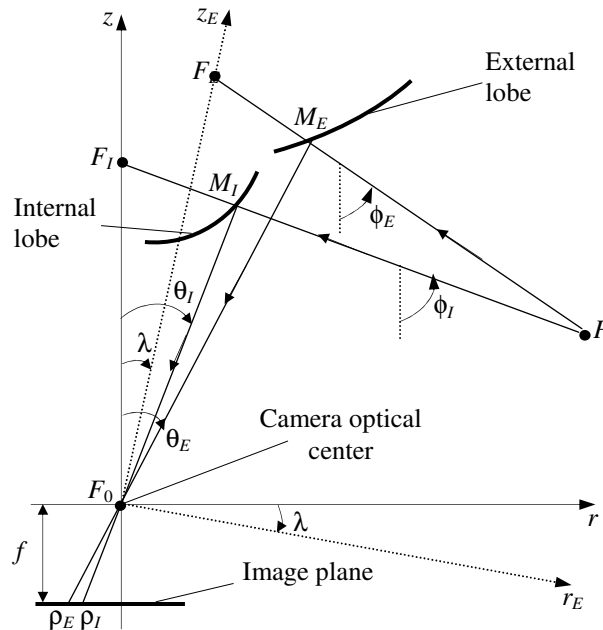


Figure 2. Radial cross section of the omnidirectional stereo vision system showing the incident and reflective light rays on the mirror emitted from a point  $P$  in space.

For a good stereo vision system it is desired that the two mirror sections have the same field of view. The field of view is defined by the minimum and maximum elevation angles. To have the same field of view for both mirror sections with hyperbolic profiles and with the optical axis of the external section aligned with the camera axis, the external section ends up with a much larger diameter than the internal section; thus, the internal image will have a much lower resolution than the external image. The error in the range measurement is proportional to the resolution of the images of both mirror sections. Therefore, it is important to have the two images with the same radial resolution, i.e., the images must have the same number of pixels in the radial direction. The double lobed mirror developed in this work solves the problem to have a low resolution in the internal image and a high resolution in the external image. The optical axis of the internal lobe hyperbole is aligned with the camera axis, while the optical axis of the external hyperbole is not aligned with the camera axis. The profile of the external section is a hyperbole rotated around point  $F_0$

by an angle  $\lambda$ . This novel solution ensures the same field of view with the same resolution of the images generated by both mirror sections.

A hyperbolic mirror is defined in the mirror coordinate system centered at focal point  $F_0$  as

$$z = c + a\sqrt{b^2 + r^2} / b, \quad (1)$$

where  $c$ ,  $b$  and  $a$  are parameters of the hyperbole, with the restriction that  $c^2 = a^2 + b^2$ . These parameters are different for the internal and external lobes. Equation (1) is valid for the internal hyperbole described in the camera coordinate system ( $F_0-rz$ ), and for the external hyperbole described in the external lobe coordinate system ( $F_0-r_Ez_E$ ).

Figure 3 presents the changes in the mirror profile for several rotation angles of the external section. From Fig. 3 it is easy to observe the decrease of the external section as the rotation angle increases. All the external section profiles shown in Fig. 3 have the focal point in the same position.

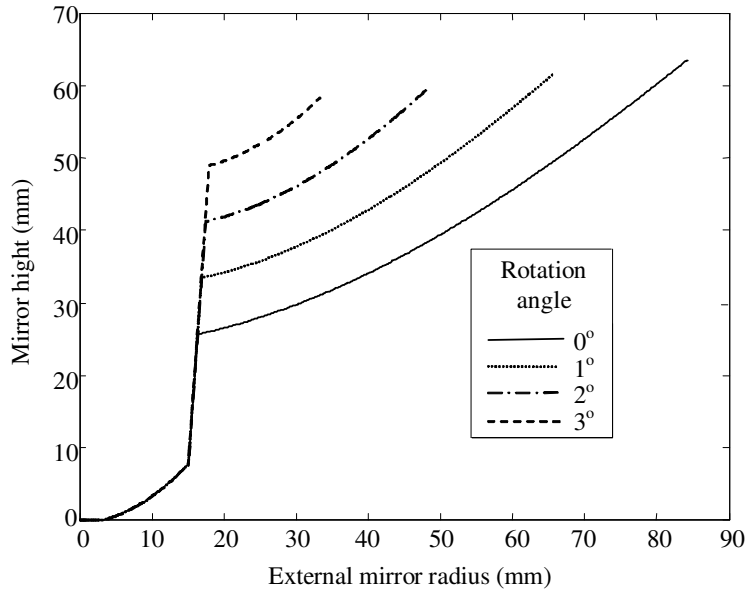


Figure 3. Change in the mirror profile for several rotation angles of the external section for the same field of view.

## 2.2. Image Formation Model

Given a point  $P$  in space as shown in Fig. 2, two light rays emitted from this point reach the mirror surface, one on the internal lobe and other on the external lobe. The incident light ray with the elevation angle  $\phi_I$  reach the internal mirror lobe at point  $M_I$  and projects onto the image at radius  $\rho_I$ . The incident light ray with the elevation angle  $\phi_E$  reaches the external mirror lobe at point  $M_E$  and projects onto the image at radius  $\rho_E$ . The equation for any incident light ray on the surface of the internal mirror lobe is

$$z = -r \cotan \phi_I + z_{FI}, \quad (2)$$

where  $z_{FI}$  is the  $z$  coordinate of point  $F_I$ . Similarly, for any incident light ray on the external lobe surface,

$$z = -(r - r_{FE}) \cotan \phi_E + z_{FE}, \quad (3)$$

where  $(r_{FE}, z_{FE})$  are the coordinates of the focal point  $F_E$ .

For any light ray reflected both from the internal and external mirror lobes the following equation holds

$$\tan \theta = \rho / f = r_M / z_M, \quad (4)$$

where  $f$  is the lens focal distance,  $\theta$  is the camera vertical angle,  $(r_M, z_M)$  are the coordinates of a point on the mirror surface, and  $\rho$  is the image radius.

The coordinates of any point lying on the internal mirror surface must obey the internal lobe profile given by Eq. (1). Also, the coordinates of any point lying on the external mirror surface must obey the external hyperbole equation given in the  $F_0-r_Ez_E$  coordinate system by Eq. (1).

Equation (5) gives the coordinate transformation from the camera to the external lobe coordinate systems.

$$\begin{bmatrix} r \\ z \end{bmatrix} = \begin{bmatrix} \cos \lambda & -\sin \lambda \\ \sin \lambda & \cos \lambda \end{bmatrix} \begin{bmatrix} r^{(E)} \\ z^{(E)} \end{bmatrix}, \quad (5)$$

where  $(r^{(E)}, z^{(E)})$  are the coordinates of a point described in the external lobe coordinate system.

### 3. CALCULATION OF RANGE

Given a point  $P$  in space, as shown in Fig. 2, the information available to calculate its coordinates in space  $(r_P, z_P)$  are the radiuses of its projection on the internal and external images ( $\rho_I$  and  $\rho_E$ ). Note that the radiuses of a point in the images are obtained through the search of correspondent points. The coordinates of point  $P$  are obtained by solving simultaneously Eqs. (2) and (3) for the incident light rays from  $P$  to each mirror lobe reflection point ( $M_I$  and  $M_E$ ).

$$\begin{bmatrix} r_P \\ z_P \end{bmatrix} = \frac{1}{(\tan \phi_E - \tan \phi_I)} \begin{bmatrix} \tan \phi_I [\tan \phi_E (z_{FI} - z_{FE}) - r_{FE}] \\ z_{FE} \tan \phi_E - z_I \tan \phi_I + r_{FE} \end{bmatrix}. \quad (6)$$

The only unknowns in Eq. (6) are the elevation angles ( $\phi_I$  and  $\phi_E$ ). Thus, to obtain the position of a point in space the tangent of the elevation angles are needed. From first optics and geometric considerations  $\tan \phi_I$  can be derived to give:

$$\tan \phi_I = \frac{2k_I \rho_I \left( f + \sqrt{f^2 + \rho_I^2} \right)}{k_I^2 (f + \sqrt{f^2 + \rho_I^2})^2 - \rho_I^2}, \quad (7)$$

where  $k_I = (c_I - a_I)/(c_I + a_I)$ . Similarly for the external mirror lobe, the same analysis results into:

$$\tan \phi_E^{(E)} = \frac{2k_E \rho_E^{(E)} \left( f^{(E)} + \sqrt{f^{(E)2} + \rho_E^{(E)2}} \right)}{k_E^2 (f^{(E)} + \sqrt{f^{(E)2} + \rho_E^{(E)2}})^2 - \rho_E^{(E)2}}, \quad (8)$$

where  $k_E = (c_E - a_E)/(c_E + a_E)$ , and  $f^{(E)}$  and  $\rho_E^{(E)}$  are respectively the focal distance and the image radius given in the external lobe coordinate system ( $F_0-r_Ez_E$ ).  $f^{(E)}$  and  $\rho_E^{(E)}$  are calculated by inverting Eq. (5) as follows

$$\begin{bmatrix} \rho_E^{(E)} \\ f^{(E)} \end{bmatrix} = \begin{bmatrix} \cos \lambda & \sin \lambda \\ -\sin \lambda & \cos \lambda \end{bmatrix} \begin{bmatrix} \rho_E \\ f \end{bmatrix}. \quad (9)$$

The elevation angle  $\phi_E$  in the coordinate system  $F_0-rz$ , is obtained from  $\phi_E^{(E)}$  as:

$$\phi_E = \phi_E^{(E)} - \lambda. \quad (10)$$

In summary, given the image radiuses of the corresponding points in the internal and external images ( $\rho_I$  and  $\rho_E$ ), using (7), (8), (9) and (10) the tangents of the elevation angles of the incident light rays are calculated and through (6) the position of the point in space is obtained. Note that in this process it is not necessary to calculate the elevation angles but only their tangents, which makes this calculation very efficient, fast and easy to be implemented in a digital computer. The derivation of the equations presented in this is section is shown in Souza Jr (2004).

### 4. PRELIMINARY ERROR ANALYSIS

To obtain range measurements with the desired accuracy the camera-mirror system need to be designed accordingly. Thus, it is very important to perform an analysis of the errors associated with the range measurements to provide information for the mirror design and for the camera specification. A simplified analytical error analysis, neglecting the radial distance between the focal points  $F_I$  and  $F_E$ , is made to provide an estimate of the expected error. Figure 4 shows

a simplified diagram of the triangulation process made with the projections of a point on the two sections of the double lobed mirror.

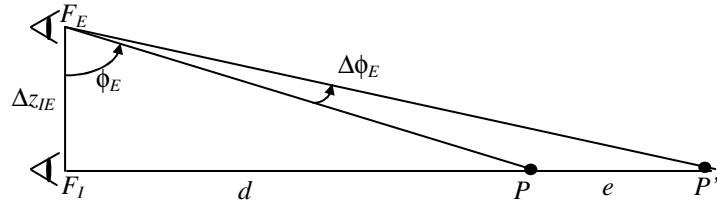


Figure 4. Simplified diagram of the triangulation process showing the error in the range measurement.

For the sake of simplicity, it is assumed that point  $P$  in space is aligned with the point of view of the internal section and the error in the range measurement is due to the error in the determination of the elevation angle for the incident light ray of the external mirror section. Thus, the error is given by the following expressions:

$$e = \Delta z_{IE} \tan(\phi_E + \Delta\phi_E) - d; \quad \tan \phi_E = \frac{d}{\Delta z_{IE}}; \quad (11)$$

where,  $d$  is the real distance of point  $P$ ,  $e$  is the error the in the range measurement,  $\phi_E$  is the corrected elevation angle,  $\Delta\phi_E$  is the error in the elevation angle, and  $\Delta z_{IE}$  is the distance between the focal points of the two sections of the mirror (points  $F_1$  and  $F_E$ ).

The error in the range measurement depends on the range measurement itself ( $d$ ), on the distance between the focal points of the two mirror sections ( $\Delta z_{IE}$ ), and on the error in the elevation angle ( $\Delta\phi_E$ ). Figure 5(a) presents the relative error in the range measurement ( $e/d$ ), for  $\Delta\phi_E$  equals to  $0,3^\circ$  as function of  $d$  for three values of  $\Delta z_{IE}$  and Figure 5(b) presents the relative error for  $\Delta z_{IE}$  equals to 150mm as function of  $d$  for three values of  $\Delta\phi_E$ .

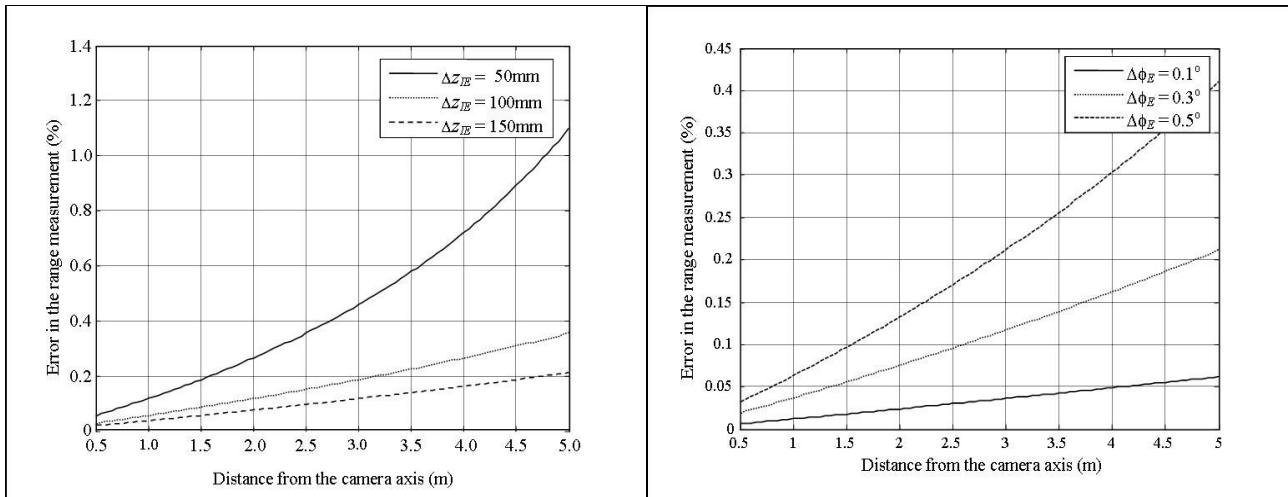


Figure 5. (a) Relative error as function of the distance from the camera axis for three values of  $\Delta z_{IE}$ , for  $\Delta\phi_E$  equals to  $0,3^\circ$ . (b) Relative error as function of the distance from the camera axis for three values of the error in the elevation angle, for  $\Delta z_{IE}$  equals to 150mm.

From Fig. 5(a) and (b) the following conclusions are obtained: (1) the error for great distances may be very large for some conditions; (2) the error in the range measurement is very sensitive to the values of  $\Delta z_{IE}$  and  $\Delta\phi_E$ ; (3) for fixed values of  $\Delta z_{IE}$  and  $\Delta\phi_E$  the error increases with the distance from the camera axis; and (4) for a fixed distance  $d$  the error increases with increasing  $\Delta\phi_E$  and with decreasing  $\Delta z_{IE}$ . The distance between the focal points of the two mirror sections is a design parameter that must be chosen to minimize the error for the desired application. The error in the elevation angle depends on the number of pixels in the internal and external images (quantization error), on the correspondence errors, on the camera sensor (CCD) resolution, and on the mirror field of view.

The results of this error analysis provide a guide to choose the main design parameters for the vision system: number of pixels in the camera CCD, field of view, distance between focal points of the two mirror sections,  $\Delta z_{IE}$ .

## 5. CALCULATION OF THE MIRROR PROFILE

The two lobes are designed to have the same field of view, which is described by the minimum and maximum elevation angles of the scene. To achieve best resolution the projection of the mirror has to occupy the whole image and to achieve equal resolution in both sections of the mirror the two images must have the same radius range, i.e.,

$$(\rho_{E,max} - \rho_{E,min}) = (\rho_{I,max} - \rho_{I,min}) \quad (12)$$

where  $\rho_{I,max}$ ,  $\rho_{I,min}$ ,  $\rho_{E,max}$  and  $\rho_{E,min}$  are the maximum and minimum image radius of the internal and external mirror lobes.

The parameters needed for the mirror design are the minimum and maximum elevation angles, the lens focal distance ( $f$ ), the maximum image radius ( $\rho_{max}$ ), the axial distance between focal points ( $\Delta z_{IE}$ ), and the maximum external radius of the mirror ( $\rho_{max}$ ). With the exception of  $\rho_{max}$ , these parameters are chosen based on the application requirements. The minimum and the maximum elevation angles and the axial distance between the focal points  $F_I$  and  $F_E$ , are chosen to obtain the desired reconstruction accuracy for a given maximum distance, see Section 4.

Geometric restrictions provide three relations between the internal and external hyperbole eccentricity,  $c_I$  and  $c_E$ , the angle  $\lambda$ , and the coordinates of focal points  $F_I$  and  $F_E$ .

$$2c_I = z_{FI} ; \quad 2c_E = \sqrt{r_{FE}^2 + z_{FE}^2} ; \quad \tan \lambda = r_{FE} / z_{FE} . \quad (13)$$

Equations (12) and (13) together with the expressions for the incident and reflected light rays with the maximum and the minimum elevation angles on the internal and external mirror lobes (Eq. 2 and 3) form a system of non-linear equations. The solution of this system results in the shapes of the internal and external mirror sections.

### 5.1. The mirror design

Based on the preliminary error analysis the main parameters for the design of the vision system are chosen. The camera has a sensor (CCD) with 1280x1024 pixels with maximum image radius equals to 3.5945mm. The 62 central pixels are discharged from the omnidirectional image resulting into 225 pixels in height for each panoramic image of the two lobes. The lens has a focal distance equals to 25mm. The mirror has a field of view that encompasses elevation view angles of the scene between 22.6° and 85°. With these parameters, the maximum error in the elevation angle resulted in 0.27°, which corresponds to the field of view of 62.4° divided by the radial number of pixels (225) in the internal and external images. Adopting a maximum relative error in the range measurements equals to 20% for great distances (about 5m), and a maximum mirror radius equals to 60mm results into a distance between the focal points of the two mirror sections,  $\Delta z_{IE}$ , equals to 150mm, and the rotation angle,  $\lambda$ , equals to 3.5067°. Note that the error is much smaller for small distances, which are the most important for robot applications. The main parameters of the mirror shape are shown in Table 1.

Table 1. Main parameters of the mirror.

Parameter	Value	Parameter	Value
$r_{FE}$	25.76mm	$z_{FE}$	420.30mm
$r_{FI}$	0.00mm	$z_{FI}$	270.30mm
$c_E$	210.54mm	$a_E$	193.61mm
$c_I$	135.15mm	$a_I$	123.79mm

Figure 6 presents a picture of the omnidirectional vision system developed. The camera is fixed in a  $xy$  table which allows translation movement with respect to the mirror. The mirror is fixed in a two degree rotational table (pitch and yaw angles) which allows the rotation of the mirror with respect to the camera. The translation and rotation movements are necessary for the system calibration.

### 5.2. Numerical analysis of the error

With the mirror designed a detail numerical analysis of the error in the range measurement is performed. Figure 7 shows the radial distance and height for all possible correspondent pixels in the internal and external images. The region of space considered for this calculation is within a distance range between 100mm and 5000mm from the axis of the mirror and with a minimum height of -850mm. Note that the camera optical center (point  $F_0$ ) is at height zero. Given

the number of pixels presented in each image and the region of space considered there are 22,594 points in Fig. 7. The positions in space of these points are calculated according to the equations presented in Section 3.



Figure 6. Picture of the omnidirectional stereo system.

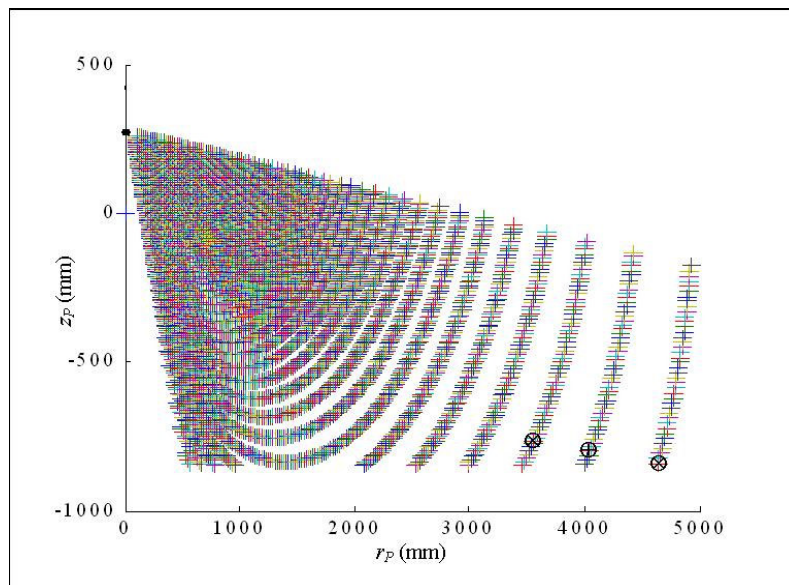


Figure 7. Position in space for all possible points determined from the vision system inside a region of the space defined by the distance between 100mm and 5000mm from the axis of the mirror and with a minimum height of  $-850\text{mm}$ .

An error analysis for the calculated position of a point in space can be performed from Fig. 7. The white areas in Fig. 7 represent points of the space that cannot be determined by the vision system due to the existence of a finite number of pixels in the camera, this is the quantization error. This quantization error may large depending on the application; however a sub pixel correspondence could be used to decrease the error. From Fig. 7 it is also possible to determine position errors due to correspondence errors. For instance, consider a point in space located at  $r_p = 4000\text{mm}$  and  $z_p = -800\text{mm}$  (point marked with  $\oplus$ ). If the correspondence is made with an error of one pixel, then the point can be thought to be locating either at  $(3600\text{mm}, -750\text{mm})$  or at  $(4600\text{mm}, -850\text{mm})$  (points marked with  $\otimes$ ).

The results of this numerical analysis agree very well with the results of the preliminary analytical analysis. It is possible to observe from Fig. 7 that the position error is a function of the position itself, i.e., the error depends on the radial distance ( $r_p$ ) and the height ( $z_p$ ) of the point. For the region of the space considered, the maximum quantization error, or the error caused by an error in correspondence of one pixel, is about 15% of the radial distance for a point located at 4000mm. The quantization error depends on the number of pixels in the images. In this case the two images have 225 pixels in height. If a smaller error is desired two options exist: to increase the number of pixels of the camera, or to perform subpixel correspondence.

## 6. CORRESPONDENCE

A fundamental problem in stereo vision is establishing the matches between image elements in the two images (correspondence problem). The epipolar constraint reduces the problem of finding correspondent points in the two images to a one-dimensional search. The epipolar constraint for catadioptric systems with hyperbolic mirrors has been studied by Svoboda et al. (1998).

The arrangement of the double lobed mirror ensures the vertical alignment of the two hyperboles, and since only one image generates the two views of the scene, the doubled lobed mirror also ensures matched epipolar lines both in the omnidirectional and panoramic images (see Fig. 8). Matched epipolar lines are desirable because efficient search methods can be used to perform stereo correspondence, thus, allowing fast and real-time three-dimensional reconstruction.

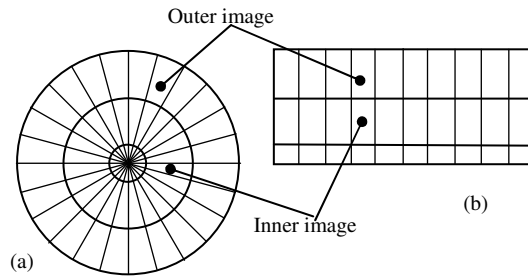


Figure 8. Epipolar geometry. (a) The epipolar lines are radial lines in the omnidirectional image. (b) When the image is projected onto a panorama the epipolar lines become vertical lines.

The panoramic image is used for the correspondence problem. Corresponding points are search in the matched epipolar lines which are the columns of the internal and external images. The horizontal edges are used as characteristics for correspondence. To quantify the similarity of corresponding pixels, the pixels intensity values at the horizontal edges positions in the original internal and external images are compared using a similarity function. The similarity function sum-of-absolute-differences (SAD) is used. A seven-pixel length by three-pixel wide window is used in the SAD. The SAD is preferred over other similarity functions for real-time applications due to its lower computational cost (Fielding and Kam, 2000). The correspondence method used is the dynamic programming (DP). Maximum and minimum disparities constraints are added to the DP to minimize the computational cost. Although the dynamic programming presents a relatively high computational cost its performance justify its use.

## 7. RESULTS

As a first step the calibration of the camera-mirror system is performed. With the camera perfected aligned with the mirror, the two images are perfectly concentric and their centers are located at the center of the omnidirectional image, also the border of the external image is tangent to the external border of the camera sensor. An iterative process to adjust the camera position and the mirror orientation is enough to perfect align the camera and the mirror.

Figure 9(a) shows an omnidirectional image acquired with the system and Fig. 9(b) shows the panoramic image obtained by projecting the omnidirectional image onto a cylinder. Four boxes are placed at about 1m around the vision system. The internal and external images in the panoramic image have 225 pixels in height and 360 pixels in length. Thus, the tangential resolution of the panoramic image is  $1^\circ$ . The horizontal edges presented in the images are used as characteristic points for correspondence and range calculation. The horizontal edges are detected by the Canny method.

Figure 10 presents the distances of the closest objects from the axis of the vision system. The vision system is located at point (0, 0) in the figure. In Fig. 10 it is possible to observe the four boxes located each one at a distance around 1000mm from the axis of the vision system. The distances of these objects detected by the system agree relatively well with the real positions.

## 8. CONCLUSIONS

An omnidirectional stereo vision system based on a double lobed mirror with hyperbolic profile was designed and tested. The system is used to give range measurements for the entirely panorama around the camera with the need for only one image.

As hyperbolic mirrors ensure a single viewpoint the incident light rays are easily found from the points of the image. This property and the perfect alignment of the images ensuring matched epipolar lines make this mirror especially suitable for real-time stereo calculations.

Although there is an error associated with the distances measured, the results show that the system is capable of

giving range measurements with the necessary accuracy for mobile robot navigation. Better accuracy could be achieved by using a camera with more pixels or by using subpixel correspondence.

The results show that the similarity function SAD associated with the dynamic programming are capable of estimating the range of the closest objects with very low computational cost. For mobile robot the closest horizontal edges (or the closest objects) are enough to provide information for safe robot navigation.

The distances of the closest objects around the vision system can be used by a mobile robot navigation system to construct a map of the environment as the robot moves around and to find the robot position in the environment. The vision system can also be used for 3D reconstruction. However, for this application a sub pixel correspondence method shall be used in order to have smaller errors in the calculated position of a point in space. Note that a relative error of 15% in the distances measured is not suitable for three-dimensional reconstruction.

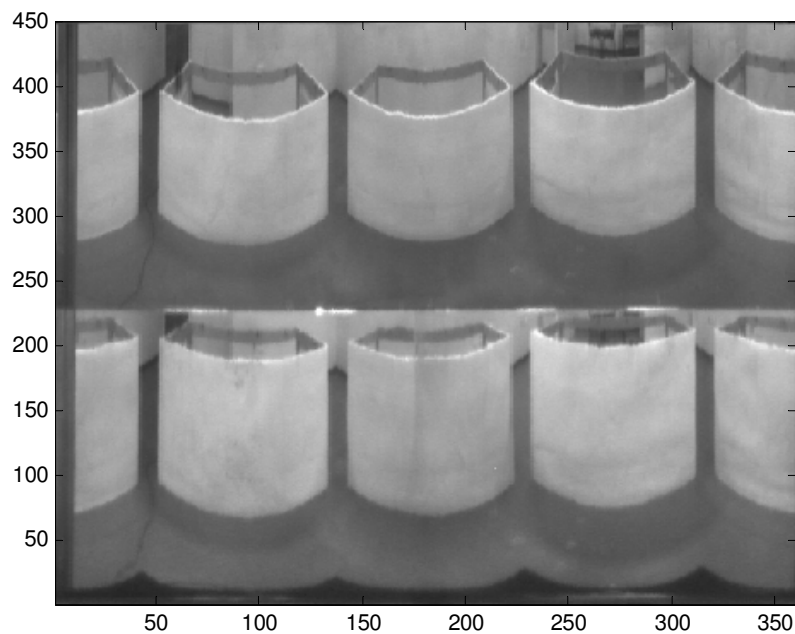
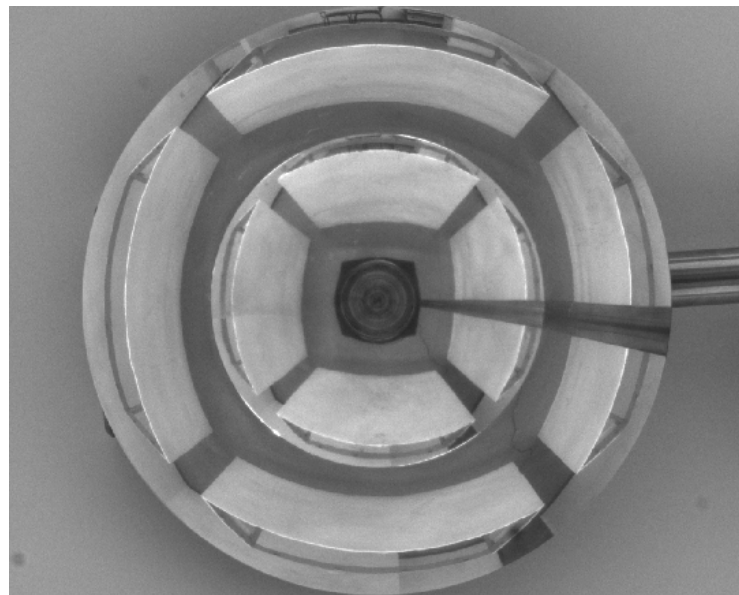


Figure 9. (a) An example of an omnidirectional image. (b) Panoramic image obtained by projecting the omnidirectional image onto a cylinder (external image up).

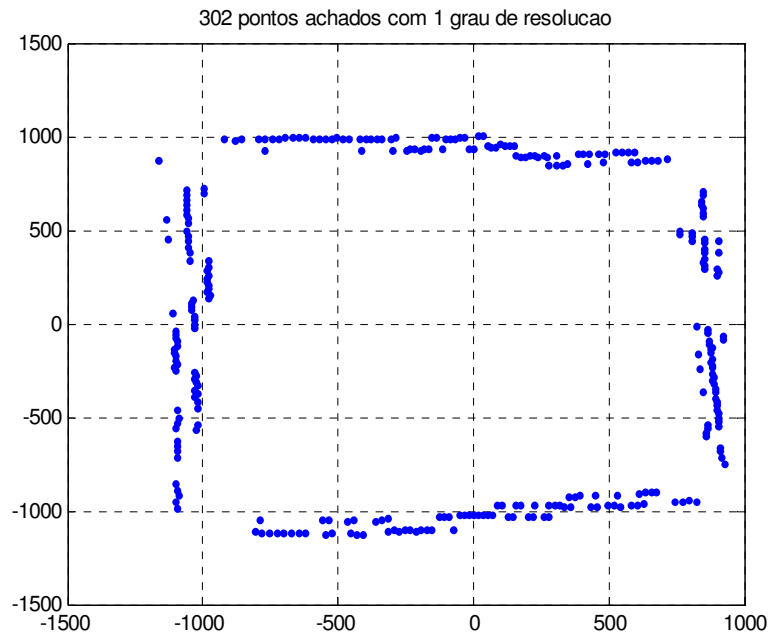


Figure 10. Distances of the closest objects from the vision system.

## 9. ACKNOWLEDGMENT

The authors would like to thank Fundação de Amparo à Pesquisa do Estado de São Paulo, Brazil, (FAPESP) for the support of this project.

## 10. REFERENCES

- Conroy, T.L., and J.B. Moore (1999). Resolution invariant surfaces for panoramic vision systems, In *IEEE ICCV'99*, pp. 392-397.
- Delahoche, L., C. Pegard, B. Marhic, P. Vasseur (1997). A navigation system based on an omnidirectional vision sensor, In *Intelligent Robots and Systems*, Grenoble.
- Fielding, G. and M. Kam (2000). Weighted matchings for dense stereo correspondence, *Pattern Recognition*, **Vol. 33**, pp. 1511-1524.
- Gaspar, J.G., C. Deccó, J. Okamoto Jr., and J. S. Victor (2002). Constant resolution omnidirectional cameras, In *OMNIVIS'02*, Copenhagen.
- Gluckman, J., S.K. Nayar, and K.J. Thoresz (1998). Real-time omnidirectional and panoramic stereo, In *Proc. of Image Understanding Workshop - IUW'98*.
- Koyasu, H., J. Miura, and Y. Shirai (2002). Recognizing moving obstacles for robot navigation using real-time omnidirectional stereo vision, *J. of Robotics and Mechatronics*, **Vol. 14**, No. 2, pp. 147-156.
- Southwell, M.F.D., A. Basu, and J. Reyda (1996). Panoramic stereo, In *ICPR*; pp. 378-382, Vienna.
- Souza Jr., J. C. de (2004). *Omnidirectional stereo vision using a double lobed mirror with hiperbolic profile*, Doctoral Thesis, Escola Politécnica da USP, 2004, (in Portuguese).
- Svoboda T., V. Padjdla, Hlavác (1998). Epipolar geometry for panoramic cameras, In *ECCV'98*, pp. 218-231, Freiburg.
- Yamazawa, K., Y. Yagi, and M. Yachida (1999). Omnidirectional imaging with hyperboloidal projection, In *IEEE/RSJ Int. Conf. Intell. Robots and Systems*.

## 11. RESPONSIBILITY NOTICE

The authors are the only responsible for the printed material included in this paper.